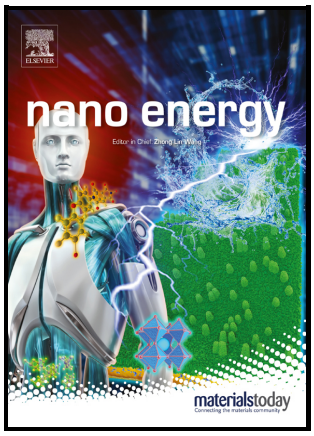

Efficient multi-physical crosslinked nanocomposite hydrogel for a conformal strain and self-powered tactile sensor

Xiangyu Zeng, Lijing Teng, Xinping Wang, Tao Lu, Weng Leng, Xujie Wu, Dan Li, Yeshuang Zhong, Xiaomin Sun, Simian Zhu, Yu Dong, Puchuan Tan, Zhu Zeng, Zuquan Hu, Zhou Li, Qiang Zheng

PII: S2211-2855(25)00028-X

DOI: https://doi.org/10.1016/j.nanoen.2025.110669

Reference: NANOEN110669

To appear in: *Nano Energy*

Received date: 2 December 2024
Revised date: 29 December 2024
Accepted date: 11 January 2025

Please cite this article as: Xiangyu Zeng, Lijing Teng, Xinping Wang, Tao Lu, Weng Leng, Xujie Wu, Dan Li, Yeshuang Zhong, Xiaomin Sun, Simian Zhu, Yu Dong, Puchuan Tan, Zhu Zeng, Zuquan Hu, Zhou Li and Qiang Zheng, Efficient multi-physical crosslinked nanocomposite hydrogel for a conformal strain and self-powered tactile sensor, *Nano Energy,* (2025) doi:https://doi.org/10.1016/j.nanoen.2025.110669

Efficient multi-physical crosslinked nanocomposite hydrogel for a conformal strain and self-powered tactile sensor

Xiangyu Zeng[1,2,3,†], Lijing Teng[1,2,3,†]*, Xinping Wang[1,2,3,†], Tao Lu[1,2,†], Weng Leng[1], Xujie Wu[1], Dan Li[1,2,3], Yeshuang Zhong[1,2,3], Xiaomin Sun[1,2,3], Simian Zhu[1,2,3], Yu Dong[1,2,3], Puchuan Tan[4], Zhu Zeng[1,2,]*, Zuquan Hu[1,2,]*, Zhou Li[4]* and Qiang Zheng[1,2,3,]*

[1] School of Biology and Engineering (School of Modern Industry for Health and Medicine), Guizhou Medical University, Guian New District, Guiyang 561113, China

[2] Key Laboratory of Biology and Medical Engineering, Immune Cells and Antibody Engineering Research Center in University of Guizhou Province, Key Laboratory of Biology and Medical Engineering, Guizhou Medical University, Guian New District, Guiyang 561113, China

[3] Engineering Research Center of Intelligent Materials and Advanced Medical Devices, School of Biology and Engineering, Guizhou Medical University, Guian New District, Guiyang 561113, China

[4] Beijing Institute of Nanoenergy and Nanosystems Chinese Academy of Sciences Beijing 101400, P. R. China

*Correspondence E-mail: ljteng@gmc.edu.cn (L.J.T); zengzhu@gmc.edu.cn; (Z. Z); huzuquan@gmc.edu.cn (Z.Q.H); zli@binn.cas.cn (Z. L); zhengqiang@gmc.edu.cn (Q.Z).

[†] These authors contributed equally to this work.

Abstract: Conductive hydrogels offer significant promise for conformal electronic skin and self-powered systems. However, developing hydrogels with multifunctionality, including stretchability, self-healing, tissue adhesion, and biocompatibility, remains a significant challenge. In this study, multiple physically crosslinked nanocomposite hydrogels were developed through the in situ doping of

poly(3,4-ethylenedioxythiophene):poly(styrenesulfonate) (PEDOT:PSS) in a Laponite® (LAP) crosslinked oligo ethylene glycol (OEG) methyl ether methacrylate copolymer. Through combined covalent and non-covalent interactions, coupled with metal ion doping, the developed conductive nanocomposite hydrogel achieved excellent stretchability (~450%), high self-healing efficiency (~95%), robust tissue force (~0.5 N/cm^2), and good biocompatibility. These features made it highly suitable for applications as a skin conformal strain sensor for human motion monitoring. In addition, it could be used as a flexible electrode in triboelectric nanogenerators, enabling tactile sensing for human–machine interactions and demonstrating its potential in self-powered electronics.

Graphical abstract

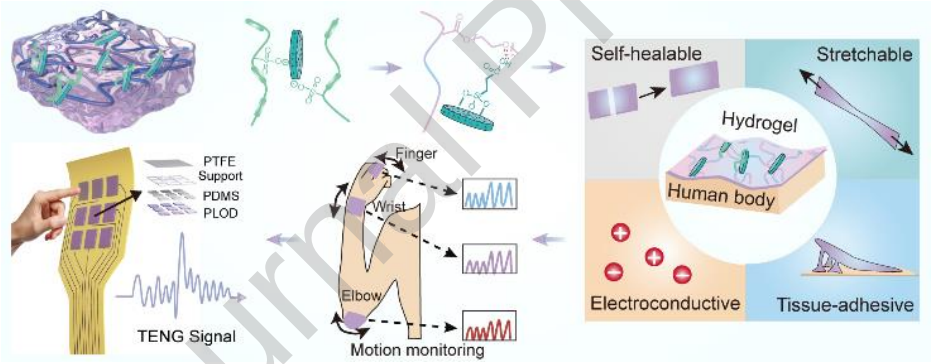

Keywords: Conductive nanocomposite hydrogel, self-healing, tissue-adhesion, strain sensor, triboelectric nanogenerator

1. Introduction

With the rise of artificial intelligence and the Internet of Things, flexible and wearable electronics have become critical in research areas such as multimodal electronic skin [1, 2], strain or pressure sensors [3], and soft robotics [4]. These

devices can mimic the performance of human skin, transforming external stimuli into electrical signals [5]. Although various candidate materials have been explored, extreme practical application contexts, such as twisting, bending, and stretching, may damage the overall electronic device. To address this issue, conductive hydrogels have been developed as versatile polymers. Their high water content, tunable mechanical performance, and similarity to the conductive mechanisms of biological systems [6] make them ideal for use in flexible and wearable electronics, including flexible/wearable sensors [7], triboelectric nanogenerators (TENGs) [8], hydrogel actuators [9], and supercapacitors [10]. Tunable mechanical performance can also provide stable conformal interfaces between electronic devices and skin, eliminating interference from motion artifacts [11]. Notably, the inherent tissue-adhesive performance of hydrogels was found to further stabilize the conformal interface between the device and skin, while reducing allergy risk [12]. In addition, the high water content and porous structure in hydrogels allow the conductive medium to rapidly spread, endowing them with improved electrical conductivity [11]. Particularly, breathable, anti-freezing, anti-drying and anti-swelling performance of hydrogel was found to better mimic the structure and functionality of dermis [2, 13-15]. However, traditional conductive hydrogels commonly suffer from inferior effective energy dissipation mechanisms, resulting in weak interfacial bonding and poor mechanical performance, making it difficult to balance mechanical performance, conductivity, and stability. As a result, it is essential to develop well-crafted designs that improve the overall functionality of conductive hydrogels, addressing challenges such as energy dissipation and interfacial bonding. This would provide a more dependable and secure solution for applications within wearable electronics.

Multi-physical crosslinked flexible nanocomposite hydrogels have emerged as a promising alternative to overcome issues associated with conventional hydrogels [16], which mainly form through noncovalent interactions [17], such as hydrogen bonding, hydrophobic, and electrostatic interactions, as well as metal coordination and π–π stacking. These noncovalent interactions are transient and can break and reform, contributing to the development of multifunctional conductive hydrogels. Laponite®

(LAP) is a disc-shaped structure 25 nm in diameter and 1 nm thick [18]. LAP-based nanocomposite hydrogels have demonstrated tunable mechanical performance, autonomous self-healing, and biocompatibility [19-21]. In previous studies, oligo ethylene glycol (OEG)-based copolymers/LAP nanocomposite hydrogels were developed through one-step free radical copolymerization, with LAP serving as a physical cross-linker for energy dissipation and providing dissociated ions for electric conduction [19]. Nevertheless, the developed nanocomposite hydrogels suffer from inadequate adhesion performance and poor electrical conductivity.

In this study, we addressed these challenges by developing a conductive nanocomposite hydrogel, denoted as PLOD, which was synthesized through the in situ gelation of OEG methyl ether methacrylate monomer crosslinked by LAP and poly(3,4-ethlenedioxythiophene):poly-(styrenesulfonate) (PEDOT:PSS) that is a promising alternative conductive polymer materials due to excellent biocompatibility [22] (Fig. 1). As shown in Fig. S1, the PLOD exhibited excellent stretchability, conductivity, self-healable and tissue-adhesive performance without external stimuli due to multi-scale interactions, which are superior to those of other LAP-based conductive hydrogels previously reported [19-21, 23, 24]. The interactions between LAP and PEDOT:PSS colloidal particles were beneficial for the dispersion and stability of the PEDOT:PSS, resulting in stretchable conductive hydrogels. As previously mentioned, PLOD could be developed as a strain sensor for monitoring human motion. The presence of numerous hydrogen bonds and electrostatic interaction in PLOD network endowed hydrogel with a robust tissue-adhesive capacity, allowing the formation of a stable conformal interface between the device and skin, facilitating high-fidelity mechanical signal transmission. The PLOD was also used as an electrode for a TENG in tactile sensing application, demonstrating significant potential for future self-powered electronics. The simple preparation and integrated functionalities of PLOD offer significant potential for expanding its application in flexible and wearable electronics.

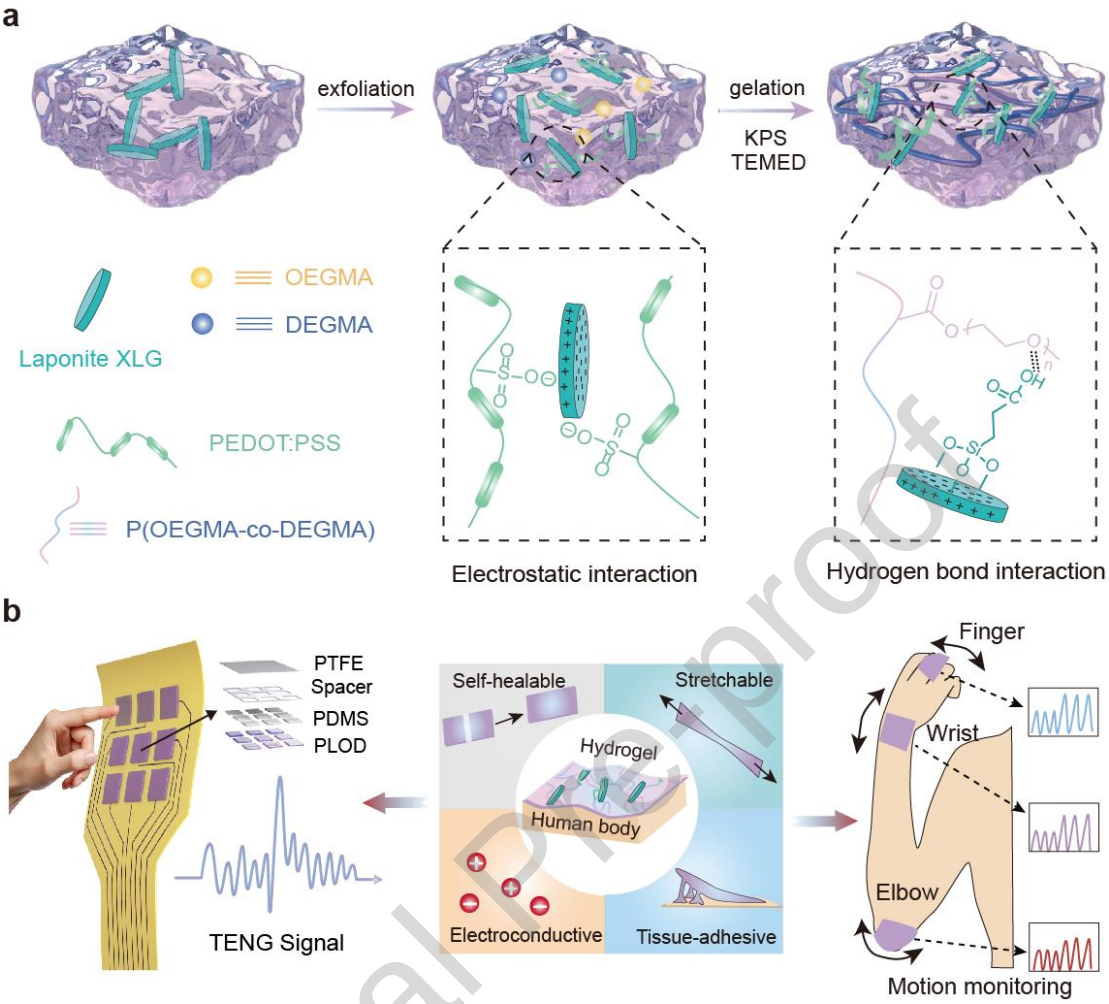

Fig. 1. Schematic diagrams of the fabrication of the PLOD nanocomposite hydrogels and application in flexible wearable strain sensors and flexible electrodes. (a) Preparation process and gelation mechanism of the PLOD nanocomposite hydrogels. (b) Application in flexible wearable strain sensors and flexible electrodes in TENGs with stretchable, self-healing, tissue-adhesive performance.

2. Experimental section

2.1. Materials

Oligo(ethylene glycol) methyl ether methacrylate (OEGMA, average molecular weight Mn = 500), di(ethylene glycol) methyl ether methacrylate (DEGMA, average molecular weight Mn = 188), *N'N'N'N'*-tetramethyl ethylenediamine (TEMED, 99%), potassium persulfate (KPS, 99%), and poly (3,4-ethylene dioxythiophene)-poly(styrene sulfonate) (PEDOT:PSS) aqueous dispersions were purchased from

Sigma-Aldrich. Laponite® clay ($Na^{+}_{0.7}[(Si_8Mg_{5.5}Li_{0.3})\ O_{20}(OH)_4]^{-}_{0.7}$, XLG) was purchased from BYK (Germany).

2.2. Synthesis and characterization of PLOD nanocomposite hydrogels

An aqueous suspension of LAP was first obtained by stirring under room temperature, then the PEDOT:PSS aqueous dispersion was added to form a homogeneous LAP/PEDOT:PSS suspension. Afterwards, OEGMA and DEGMA monomers were subsequently added to obtain a homogeneous suspension in an ice-water bath. The initiator KPS (0.2 w/v%) was introduced under nitrogen bubbling for 5 min to eliminate dissolved oxygen, followed by the addition of accelerator TEMED (0.1 w/v%) to the solution. The resulting solutions were then sealed and polymerized for 24 h at room temperature to form PLOD hydrogels. Rheological tests were conducted using an Anton Paar MCR302e rheometer (Austria) with a 25 mm diameter parallel plate. The geometries of PSS, PEDOT, OEG methyl ether methacrylate monomer were optimized using Gaussian 16 software [25] at the B3LYP-D3(BJ)/6-311++G(d,p) level of theory. The molecular electrostatic potentials (MEPs) of corresponding molecules were calculated with the Multiwfn program, using a 0.001 a.u. grid isodensity surface at the same level [26]. VMD software was utilized to visually depict the MEP maps and the highest occupied molecular orbital (HOMO) and lowest unoccupied molecular orbital (LUMO) diagrams of corresponding molecules [27]. FTIR spectra were recorded between 4000 and 400 cm^{-1} using a Nicolet iS50 FTIR spectrometer (USA). The elemental compositions and distribution maps were obtained using energy–dispersive spectroscopy (EDS, Netherlands). Thermogravimetric analysis (TGA) was conducted using PerkinElmer Instruments (China), ranging from 25°C to 800°C at a rate of 10°C/min.

2.3. Mechanical testing

A universal testing machine (MARK-10, USA) was used to determine the mechanical performance of PLOD. Rectangular specimens, measuring 10 mm in width and 1 mm in thickness, were prepared for uniaxial tensile testing conducted at

an elongation rate of 100 mm/min. The slope of the stress–strain curve between 5% and 15% strain was determined as the elastic modulus. The toughness was determined by integrating the area under the stress–strain curve [28].

2.4. Self-healing performance measurements

One PLOD was stained with rhodamine B, while the other was free of rhodamine B. The two PLOD were placed in contact for 30 s at 25°C and 75% humidity, then stretched without external stimulation, and the self-healing performance was macroscopically observed under UV irradiation [29]. During the self-healing process, no additional stimulus was applied. The PLOD, light diodes, and power supply were connected to form a series circuit. The PLOD was cut and healed, and the brightness of the light diodes was recorded [7]. The resistance change of PLOD before and after healing was also quantitatively assessed to determine the electrical recovery performance [30]. Before dynamic viscoelastic measurement, strain sweep curves were obtained by increasing the shear strain from 0.01% to 2000% to identify the linear viscoelastic region, characterized by the storage modulus independent of shear strain. The dynamic strain curves were generated at 1% and 3000% strain over 100 s intervals, to record both the storage modulus (G') and loss modulus (G'') [31]. In addition, rectangular PLOD specimens were cut into two pieces and then joined together for 24 h, and the self-healed PLOD specimens were assessed by a MARK-10 instrument (USA) [32].

2.5. Adhesive measurements

The adhesive performance of PLOD was determined by lap shear tests using a MARK-10 [33]. Square PLOD nanocomposite hydrogel specimens (20 × 20 × 1 mm) were affixed between two substrates (pigskin, copper, PDMS, PTFE, and PE) and stretched at 100 mm/min. In addition, the peeling test was performed to evaluate adhesive toughness, quantified by the average peel force normalized by the width [34].

2.6. In vitro cytotoxicity assays

An extract concentration of 1 mg/mL was prepared by soaking PLOD in Dulbecco's Modified Eagle Medium (DMEM, Gibco) for 24 h at 37°C. A 500 μL suspension of L929 mouse fibroblast cells, containing 10,000 cells per well, was seeded into a 24-well plate and incubated at 37°C with 5% CO_2. After the L929 cells adhered to the plate, the medium was removed and replaced with PLOD extract. Then, cell viability was assessed using a CCK-8 kit on days 1 and 3, according to the manufacturer's guidelines. The cells were stained with Calcein-AM/propidium iodide for 15 min and observed using a Nikon AX laser scanning confocal microscope (Japan) for fluorescence imaging.

2.7. Electrical measurements

The conductivity of PLOD was measured by a CS350M electrochemical workstation (CORRTEST, China) with electrochemical impedance spectroscopy (EIS). Copper sheets were used to secure the two extremities of PLOD, ensuring a strong connection between PLOD and electrodes of electrochemical workstation. The conductivity was determined based on the following equation [11]:

$$\text{Conductivity}=\frac{l}{RS}$$

where l denotes the effective length, R is the bulk resistance, and S represents the cross-sectional area of PLOD.

The resistivity changes rates ($\Delta R/R_0$) were determined to assess the sensing performance of PLOD. The volt-ampere method was used to determine $\Delta R/R_0$ based on a high-precision linear motor (Y400TA100-600, Beijing Aerospace Precision Instrument Technology Co., Ltd., Beijing, China) and an oscilloscope with four analog channels (MSO44, Tektronix, Beaverton, Oregon, USA). The relative change in resistance was calculated based on the following equation:

$$\frac{\Delta R}{R_0}=\frac{R-R_0}{R_0}=\frac{V-V_0}{V_0}$$

where V and V_0 represent the voltage values at the two ends of PLOD hydrogel following and preceding the application of strain, respectively. The sensitivity of the PLOD hydrogel sensor was assessed using the gauge factor (GF), as follows:

$$GF=\frac{\Delta R/R_0}{\varepsilon}$$

In addition, Fig. S2 showed the assembly and test of PLOD sensor. In brief, the rectangular PLOD was first adhered to the movement site, such as index finger. Then, one end of the copper wire connected to the surface of PLOD, the other end connected to divider resistance to form a voltage-dividing circuit, oscilloscope connected to the two ends of PLOD hydrogel to record the voltage value, DC power as a power supply for this test circuit, and finally, the PLOD sensor was assembled to complete test. In the process of test, tape was utilized to immobilize both ends of copper wire to prevent copper wire from falling off. With respect to other motion monitoring, the only diversity was that moving parts and tape removed from the assembly.

The output performance of the TENG was quantified and documented using the previously mentioned linear motor and oscilloscope, and an electrometer (Model 6517B, Keithley Instruments, Inc., Cleveland, OH, USA). The performance of the TENG array was measured and recorded by a multi-panel measurement system switch (Model 3706A-S, Keithley) and an 8-channel oscilloscope (Model MSO58B, Tektronix).

2.8. Circuitry in human–machine interaction applications

An Arduino UNO R3 (Somerville, MA, USA) was employed for signal acquisition and processing, and Arduino's integrated ADC was used to establish the trigger signal threshold. The decision-making process entailed programming that compared the amplitude of the input signal against the established threshold, after which the appropriate action was executed.

2.9. Statistical analysis

All experimental quantitative data were expressed as mean and standard deviation. The experimental data were analyzed by one-way ANOVA and expressed as mean ± SD, with $P < 0.05$ considered statistically different.

3. Results and discussion

3.1. Preparation and characterization of PLOD nanocomposite hydrogels

In this study, PLOD nanocomposite hydrogels were developed through in situ gelation of OEG methyl ether methacrylate monomer crosslinked by LAP and PEDOT:PSS. Molecular electrostatic potential (MEP) maps, as well as HOMO and LUMO orbital diagrams, were used to estimate the molecular reactivity and electron transfer mechanisms, which provided valuable insights into molecular reactivity and intermolecular interactions [35]. The HOMO energy level can be used to quantify the electron-donating tendency of a molecule, while the LUMO energy level can be used to indicate its electron-accepting ability, which performance is crucial for revealing electron dynamics. Based on the B3LYP-D3(BJ)/6-311++G(d,p) level-optimized geometric structures of OEG methyl ether methacrylate monomer, PEDOT, and PPS molecules obtained from the Gaussian16 software, Multiwfn program was used to calculate corresponding MEP, HOMO and LUMO orbital, and VMD software was utilized to visually represent the MEP maps and HOMO–LUMO orbital diagrams, which is in favor of understanding the characteristics and reactivity of OEG methyl ether methacrylate monomer, PEDOT, and PSS. With respect to the MEP maps, the red-colored areas denote positive electrostatic potential and the blue-colored areas indicate negative electrostatic potential. Fig. 2a showed the MEP maps and HOMO–LUMO orbital diagrams for the stable structures of OEG methyl ether methacrylate monomer. It was found that the ethoxy groups in OEG, which were rich in lone electron pairs, acted as electron donors, contributing to the formation of hydrogen bonds with LAP. As illustrated in Fig. 2b and 2c, the PEDOT molecule was negatively charged with abundant vacant orbitals, while the PSS molecule contained delocalized π electrons and exhibited a positively electrostatic potential due to strong electron-withdrawing ability of sulfonic acid group, leading to strong Coulombic interactions between the two molecules. The interactions between the OEG polymer backbone and PEDOT:PSS molecules primarily involved the hydrogen bonding and π–π interactions. Delocalization of weak-bound electrons in molecular orbitals is in favor of charge transfer, leading to improved electric conductivity [36]. Moreover, the

hydrophilic pores facilitated the diffusion of the conducting medium through the PLOD matrix.

The OEG-based copolymers containing short oligo(ethylene glycol) sidechains exhibited lower critical solution temperature (LCST) behavior in aqueous medium, and LCST behavior could be finely adjusted through the copolymerization of oligo(ethylene glycol) (meth)acrylates [37]. As shown in Fig. 2d, for the 30 w/v% total monomer concentration, LCST with OEGMA and DEGMA molar ratio close to 4:1 was about 50°C, while LCST with an OEGMA and DEGMA molar ratio close to 1:4 was about 34°C, indicating that the formed copolymer was no longer miscible with water at 34°C, which was not conducive to the formation of hydrogen bonds within the PLOD network. Therefore, OEGMA/DEGMA molar ratio of 4:1 was chosen for the follow-up study. As shown in Fig. S3, a critical monomer concentration was required to form a stable PLOD. At a total monomer concentration of 10 w/v%, the reaction product could flow freely. However, a monomer fraction of 20 w/v% led to gelation, which was confirmed by the inverted vial test. The formed PLOD remained very weak until reaching a monomer fraction of 25 w/v%, where a more rigid network formed. In addition, the reactive precursor could be molded into PLOD with different shapes, including a square, circle, heart, and star (Fig. S4). As shown in Fig. 2e, new absorption peaks at 1577 and 1541 cm^{-1}, resulting from PEDOT:PSS[38], were clearly observed in PLOD compared with OEGMA-co-DEGMA copolymer (OD) and LAP crosslinked OEGMA-co-DEGMA copolymer (LOD) (Fig. 2e). These peaks corresponded to C–H bonds in the thiophene rings of the PEDOT chains. In addition, an obvious characteristic peak at 980 cm^{-1}, associated with LAP, was assigned to the stretching vibrations of Si–OH and Si–O [18]. These results demonstrated that PEDOT:PSS and LAP were successfully introduced into the OEG copolymer network. Furthermore, EDS analysis revealed the presence of S and Si from PEDOT:PSS and LAP in PLOD, respectively (Fig. 2f). According to EDS-mapping analysis (Fig. 2g), the uniform distribution of C, O, S, and Si in PLOD could be observed, indicating the good dispersion of LAP and PEDOT:PSS in the OEG copolymer network.

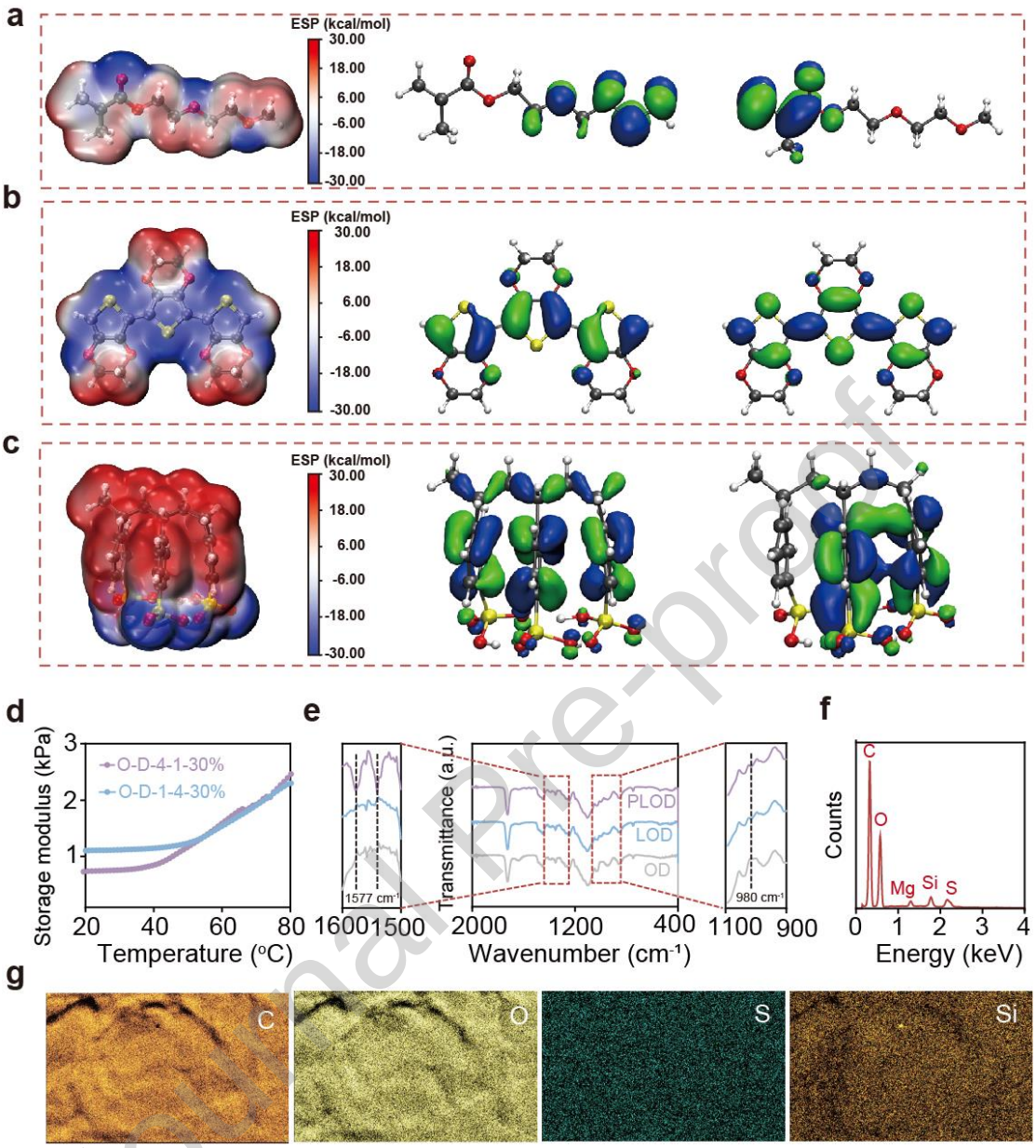

Fig. 2. Preparation and characterization of the PLOD conductive nanocomposite hydrogels. MEP, HOMO, and LUMO orbital diagrams of (a) OEG methyl ether methacrylate monomer; (b) PEDOT, and (c) PSS. (d) Temperature sweep curve of the OEG copolymer with different OEGMA/DEGMA molar ratios. (e) FTIR spectra of OD, LOD, and PLOD. (f and g) EDS and mapping analysis of PLOD for the distribution of C, O, S, and Si in the same region.

3.2. Mechanical and self-healing performance of PLOD nanocomposite hydrogels

Flexible nanocomposite hydrogels serve as promising alternatives to traditional rigid materials due to their parallel elastic modulus and stretchable performance [39].

These properties help address the mismatch between the elastic modulus of rigid sensors and soft physiological tissues while also mitigating skin irritation through conformal contact, which is crucial for wearable electronics [40]. In this study, the reactive precursor became sticky with increased LAP content from 1 to 2.5 w/v%, and the reactive precursor was nonuniform. Therefore, 1 w/v% LAP was chosen for the follow-up study. First, uniaxial tension curves were obtained to investigate the effects of OEGMA and DEGMA content on stretchable performance of LAP crosslinked hydrogel. Samples were denoted as LOD-x, where x is the total monomer mass percent of OEGMA and DEGMA with corresponding molar ratio of 4:1. As shown in Fig. 3a, the tensile performance of LOD was dependent on OEGMA and DEGMA content. LOD35 exhibited weak fracture strain, with the elastic modulus increasing from 5 to 15 kPa as OD content varied from 25 to 35 w/v% (Fig. 3b). The fracture energy values showed no significant differences (Fig. 3c). Given the fracture strain and elastic modulus, the LOD35 was chosen as follow-up experiment. Subsequently, the effect of PEDOT:PSS concentration on PLOD tensile performance was further explored. Samples were denoted as P-x, where x is the volume fraction of PEDOT:PSS. As shown in Fig. 3d-3f, PLOD with P2.5 exhibited improved fracture strain (~450%), elastic modulus (~12.5 kPa) and toughness (~1.54 MJ/m^3), which may be attributed to the fact that LAP can interact with the OEG methyl ether methacrylate copolymer, redistributing the applied stress and delaying the complete fracture of PLOD [19]. In addition, multi-scale interactions between PEDOT:PSS and LAP increased the physical cross-linked density, which endowed PLOD with effective energy dissipation during the stretching process, which further contributed to stretching performance [21].

In addition to satisfactory stretching performance, it was important to endow conductive hydrogels with self-healing performance, as flexible wearable strain sensors may encounter friction or damage during actual application, leading to malfunctions and shortening their lifespan [41]. In this work, the favorable self-healing performance of PLOD was confirmed by macroscopic, dynamic strain scanning, tensile, and resistance recovery measurements. As shown in Fig. 3g, PLOD

with P2.5 cut by a shaving blade achieved spontaneous self-healing, demonstrating excellent self-healing performance. Considering application in flexible electronics, the electroconductivity of PLOD before and after self-healing was also explored. As shown in Fig. S5, the PLOD could illuminate light diodes in a series circuit. The LED was powered off when PLOD was cut, and the LED illuminated again after PLOD self-healing. As shown in Fig. 3h, when PLOD was disrupted, noncovalent interactions on the edge of the crack were also broken. However, due to their dynamic and reversible performance, they could achieve recovery in a short time to trigger healing. Dynamic strain sweep was performed to further quantitatively determine the self-healing performance of PLOD. As shown in Fig. S6, the strain sweep curves suggested that the value of G' was significantly larger than that of G" in the range of 0.01–1300%, indicating the stable structure within PLOD. However, a critical point was observed at 1300% shear strain, indicating the collapsed structure. When the shear strain was further increased to 3000%, G' and G" both decreased dramatically, indicating the complete disruption of PLOD network. Subsequently, dynamic strain sweep was performed to further determine the self-healing performance of PLOD. As shown in Fig. 3i, G' of the PLOD was smaller than G" under 3000% strain, indicating a damaged network; however, G' and G" could quickly recover to their original state when the shear strain reverted to 1%. Fig. 3j showed the stress–strain curves of PLOD after self-healing for 24 h at 25°C and 75% humidity. The ultimate strain of healed PLOD could reach 380% compared with the initial 400%, yielding a high self-healing efficiency of 95%. Finally, the electrical recovery performance of PLOD was determined. When PLOD was cut, the resistance instantly increased to infinity. After self-healing, the resistance of PLOD could recover its initial value within 1.8 s (Fig. 3k). In conclusion, the developed PLOD displayed excellent self-healing performance, which is crucial for maintaining its original stable performance in applications where mechanical damage may occur.

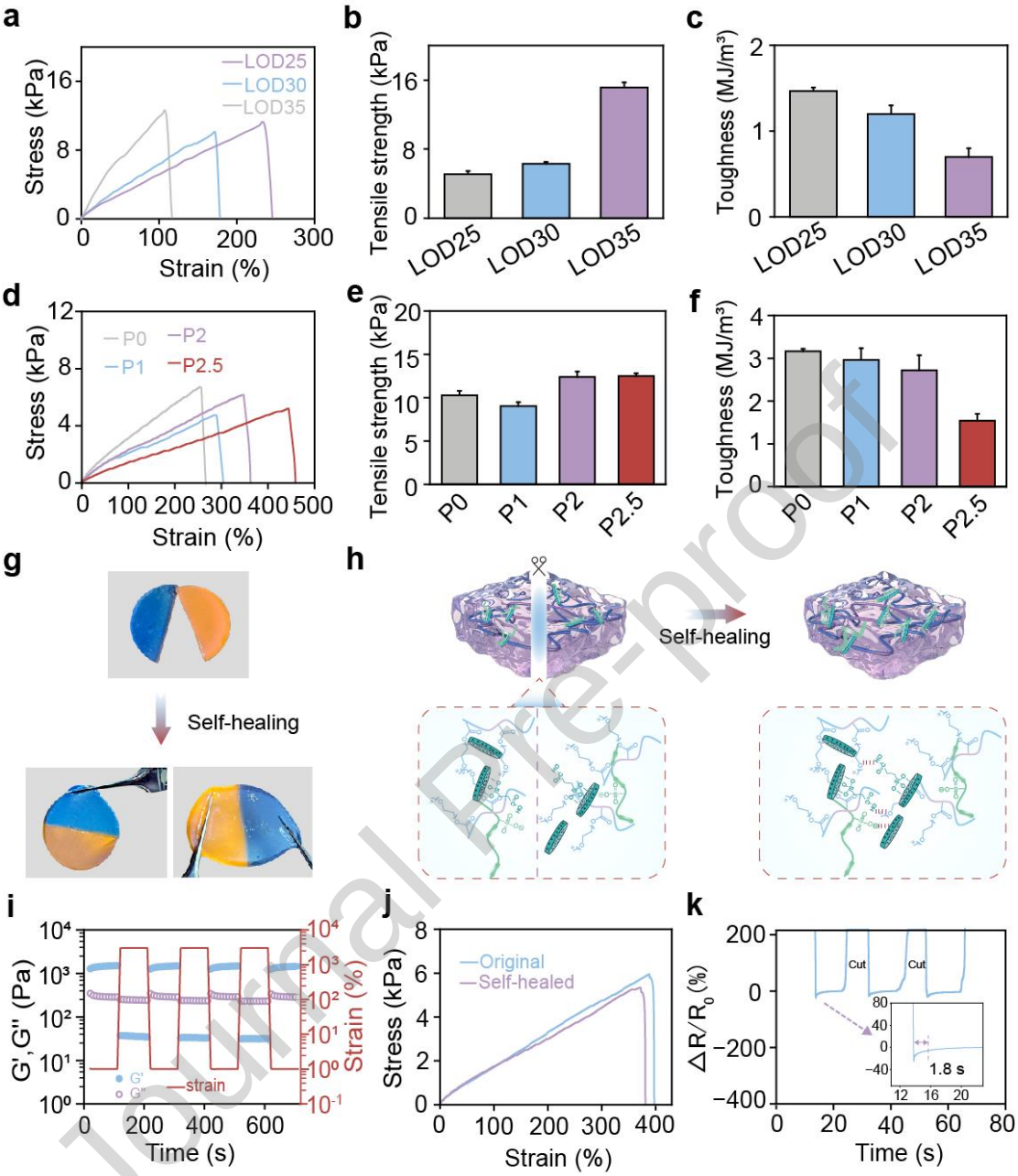

Fig. 3. Tensile and self-healing performance of PLOD. (a) Tensile stress–strain curves, (b) tensile strength, and (c) toughness of LOD. (d) Tensile stress–strain curves, (e) Tensile strength, and (f) toughness of PLOD. (g) Digital photograph showing self-healing. (h) Self–healing mechanism of PLOD. (i) Dynamic modulus of PLOD under alternating strain. (j) Tensile stress–strain curves of the original and healed PLOD. (k) Resistance recovery of PLOD under cutting-healing cycles.

3.3. Adhesive performance and cytocompatibility of PLOD nanocomposite hydrogels

Hydrogels with good adhesive performance are indispensable for wearable electronics, eliminating the need for additional bandages or tape [42]. These hydrogels would also provide reliable conformational contact with soft physiological tissues, helping to reduce interfacial resistance and gather stable signal output. As shown in Fig. S7, the PLOD exhibited strong adhesive performance, as evidenced by the firm adhesion of the heart, liver, spleen, lungs, and kidneys of Sprague-Dawley (SD) rats. In addition, PLOD could adhere to human skin and easily peel off without any residue, and no irritation or allergic reactions were observed (Fig. S8). As shown in Fig. 4a, PLOD displayed excellent adhesion to hydrophobic or hydrophilic surfaces, including human skin, copper, PDMS, PTFE, and PE.

Lap shear tests were conducted to determine the adhesive force of PLOD toward porcine skin and varied polymer surfaces (Fig. 4b), with the adhesive force dependent on the interfacial interaction force and intermolecular forces within the hydrogel [43]. In terms of intermolecular forces within PLOD, LAP could interact with the OEG methyl ether methacrylate copolymer through hydrogen bonding, helping to relax the applied stress and increase the adhesive force [44]. In addition, multi-scale interactions between PEDOT:PSS and LAP increased the physical cross-linked density, further improving cohesion within the PLOD network, and effective energy dissipation during the stretching process was beneficial for improved adhesive performance [20, 24]. As shown in Fig. S9, PLOD with LOD30 samples displayed the highest adhesive force values, possibly due to decreased cohesive forces within PLOD with increasing OEG methyl ether methacrylate copolymer content. At this point, the silicon hydroxyl groups in PLOD were consumed, and the number of exposed silicon hydroxyl groups that could interact with the substrates decreased, resulting in poor adhesion between PLOD and the substrate. In addition, excessive OEG methyl ether methacrylate copolymer content possibly affected the balance between adhesion and cohesion, leading to weak adhesive force. As shown in Fig. 4c, all PLOD samples displayed equivalent adhesive force to porcine skin when the concentration of PEDOT:PSS was increased from P0 to P2.5. Considering mechanical and adhesive performance, PLOD with P2.5 was chosen for subsequent application assessment.

Fig. S10 presents the optimized PLOD, which displayed equivalent adhesive performance after three cycles of adhesion on pigskin. The adhesive force of PLOD to copper, PDMS, PTFE, and PE was also quantitatively evaluated (Fig. 4d). The stable adhesion of PLOD to various substrates was mainly attributed to the multi-scale interactions between PLOD and substrate (Fig. 4e). The ethoxy, hydroxyl, and conjugate groups in PLOD facilitated the formation of multi-scale interactions with the substrate interface. Apart from lap shear tests, single side attached test between PLOD and pigskin was further performed. Because the adhesive force is noticeably higher than the bulk mechanical performance of PLOD, resulting in PLOD breakage before the single side adhesive interface separation. However, Fig. S11 showed that PLOD with P2.5 displayed the longest pulling time, it also indirectly proves that PLOD with P2.5 displayed better single side tissue adhesion performance.

The cytocompatibility of PLOD was tailored to meet the needs of flexible and wearable electronics while minimizing the risks of inflammatory or anaphylactic reactions [45]. As shown in Fig. 4f, few dead L929 cells were observed in the live/dead staining test. CCK-8 quantitative analysis indicated no significant difference in cell proliferation activity between the PLOD and control groups on day 1. On day 3, the proliferation activity of PLOD cell group slightly exceeded that of the control group (Fig. 4g), thus demonstrating the excellent biocompatibility of PLOD.

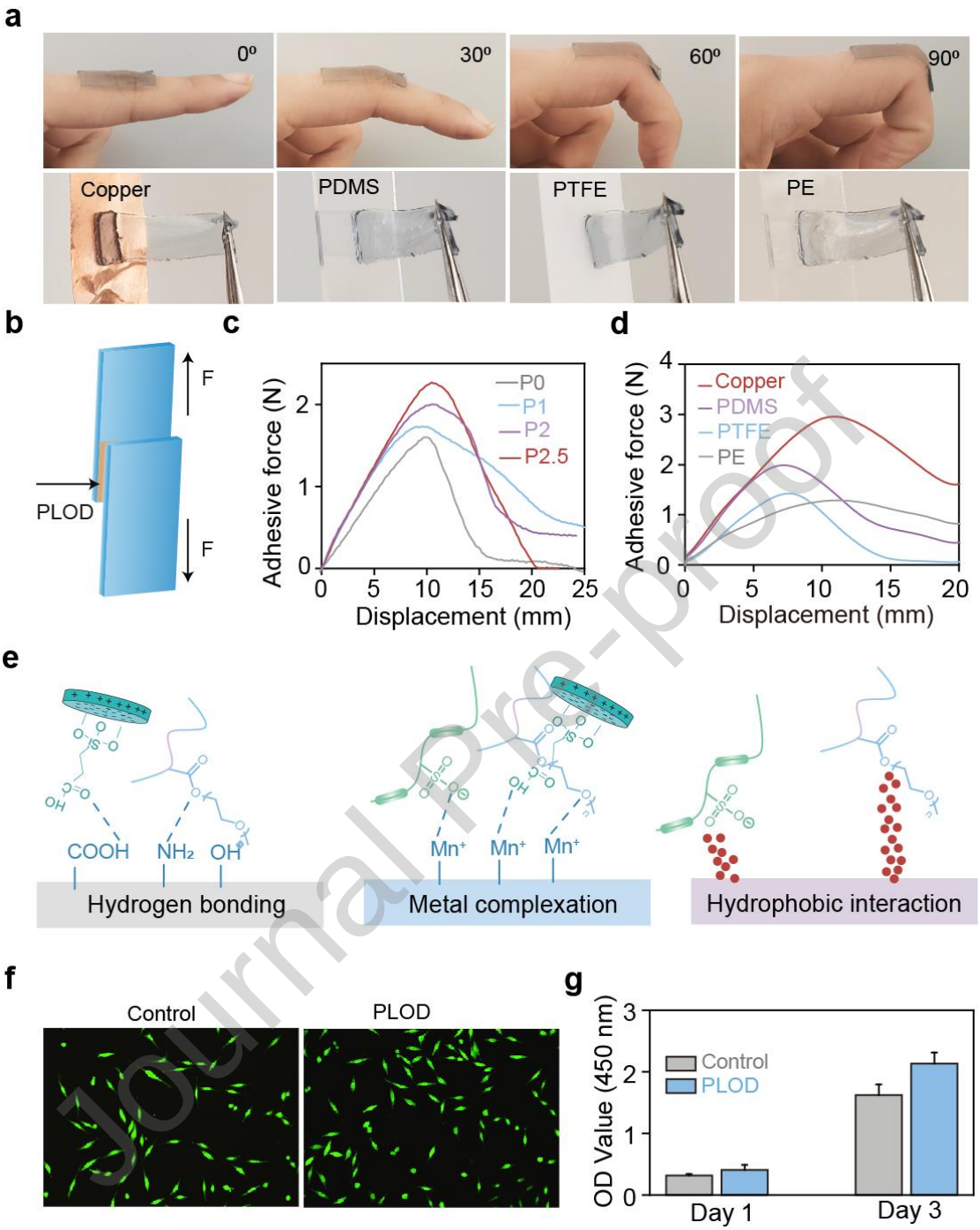

Fig. 4. Adhesive performance and cytocompatibility of PLOD. (a) Photographs of PLOD nanocomposite hydrogels adhered to biological tissue surfaces, metal, and polymer substrates. (b) Schematic diagram of the lap shear test. (c) Representative force–displacement curves for pigskin. (d) Representative force–displacement curves for copper, PDMS, PTFE, and PE substrates. (e) Adhesive mechanism of PLOD. (f) Fluorescence live/dead staining images of L929 cells co-cultured with PLOD extract. (g) OD value at 450 nm L929 cells co-cultured with PLOD extract.

3.4. Human motion detection application of PLOD nanocomposite hydrogels

The PLOD strain sensor demonstrated significant potential for detecting diverse human movements due to its excellent self-healing, stretchability, biocompatibility, conductivity, and resistance change rate. Notably, due to its tissue-adhesive performance, PLOD could directly adhere to body surfaces to detect signals, and cyclic adhesion allowed PLOD to serve as a reusable sensor. In natural skin, electrical signal conversion primarily relies on ion transfer through ion channels. Similarly, LAP could be completely exfoliated in deionized water with dissociated sodium ions, resulting in a negatively charged disk surface and hydrous oxides, enhancing the conductive network [19, 46]. In addition, the interactions between LAP and PEDOT:PSS colloidal particles were in favor of the dispersion and stability of PEDOT:PSS, further contributing to enhanced electric conductivity [20, 21]. Hence, PLOD possesses ionic conductivity from LAP and electronic conductivity from PEDOT:PSS. As shown in Fig. 5a, conductivity determined from electrochemical impedance spectroscopy (Fig. S12) increased from 0.5 to 0.7 mS/cm as PEDOT:PSS volume fraction increased from P0 to P2.5. However, further increases in PEDOT:PSS concentration resulted in heterogeneous PLOD (Fig. S13), which led to inferior conductivity. Fig. S14 showed that conductivity is about 0.6 mS/cm as PEDOT:PSS volume fraction increased to P50. This behavior at low electrolyte concentrations indicated surface charge-dependent ionic conductance and typical nanofluidic ion transport behavior [19].

The resistance of PLOD varied with deformation, indicating its potential capability to transform mechanical changes into electrical signals. Fig. 5b and Fig. 5c illustrated the resistivity change rates of PLOD across various strain cycles. During PLOD deformation, the specimen elongated, restricting ionic transport and consequently increasing the bulk resistance. Moreover, PLOD sensor consistently provided accurate, stable, and repeatable responses across various strain magnitudes. The sensor accurately reflected the deformation rate of PLOD (0.1–2.0 Hz) with no significant fluctuations in the electrical signal (Fig. S15), these two data can cover the

application range. In addition, the GF was found to increase the electrical sensitivity of the PLOD to strain (Fig. 5d). With a GF of 0.31 and a broad strain range from 10% to 300%, the sensor displayed excellent linear response behavior, demonstrating its potency as a strain sensor. Considering the maximum strain of human skin of 75% [11], repeated strain sensing experiments at 100% strain were performed with 1.5 Hz of frequency to assess long-term durability, and the resistance change remained relatively stable over 12000 cycles (Fig. 5e), indicating its suitability for long-term use as a strain sensor.

Considering the stable and efficient electronic responses of PLOD sensor under deformation, its potential as an electronic skin for monitoring various human motions was further investigated. Fig. 5f and Fig. 5g show that the PLOD, when applied to a finger and elbow, exhibited sharp and rapid resistance changes corresponding to the bending angles of motion. Furthermore, the movement signals of each joint were highly similar, demonstrating the excellent recoverability and sensitivity of PLOD (Fig. S16). The PLOD was also affixed to a volunteer's finger (Fig. 5h) and elbow (Fig. 5i) for repeated bending strain sensing experiments. The electronic skin sensor consistently detected motion signals over multiple cycles, demonstrating its long-term stability. Therefore, PLOD could be employed as a reusable wearable sensor to monitor subtle human movements for personal healthcare. Notably, PLOD could adhere to the thyroid notch to monitor swallowing behavior, with clear signals gathered during a volunteer's drinking activity (Fig. 5j). Similarly, PLOD could monitor frowning behavior through different signal strengths (Fig. 5k). Finally, PLOD exhibited significant compressibility and deformability (0.3–1 N), with changes in electrical properties under external force (Fig. S17). In summary, the PLOD sensor could differentiate movement types by analyzing the shape, height, and width of signal. The subtle variations in signals for identical movements were primarily attributed to disparities in motion amplitude. The PLOD, designed as a flexible strain sensor, showed significant potential for monitoring both large-scale and small human movements, enhancing human motion tracking and healthcare analysis.

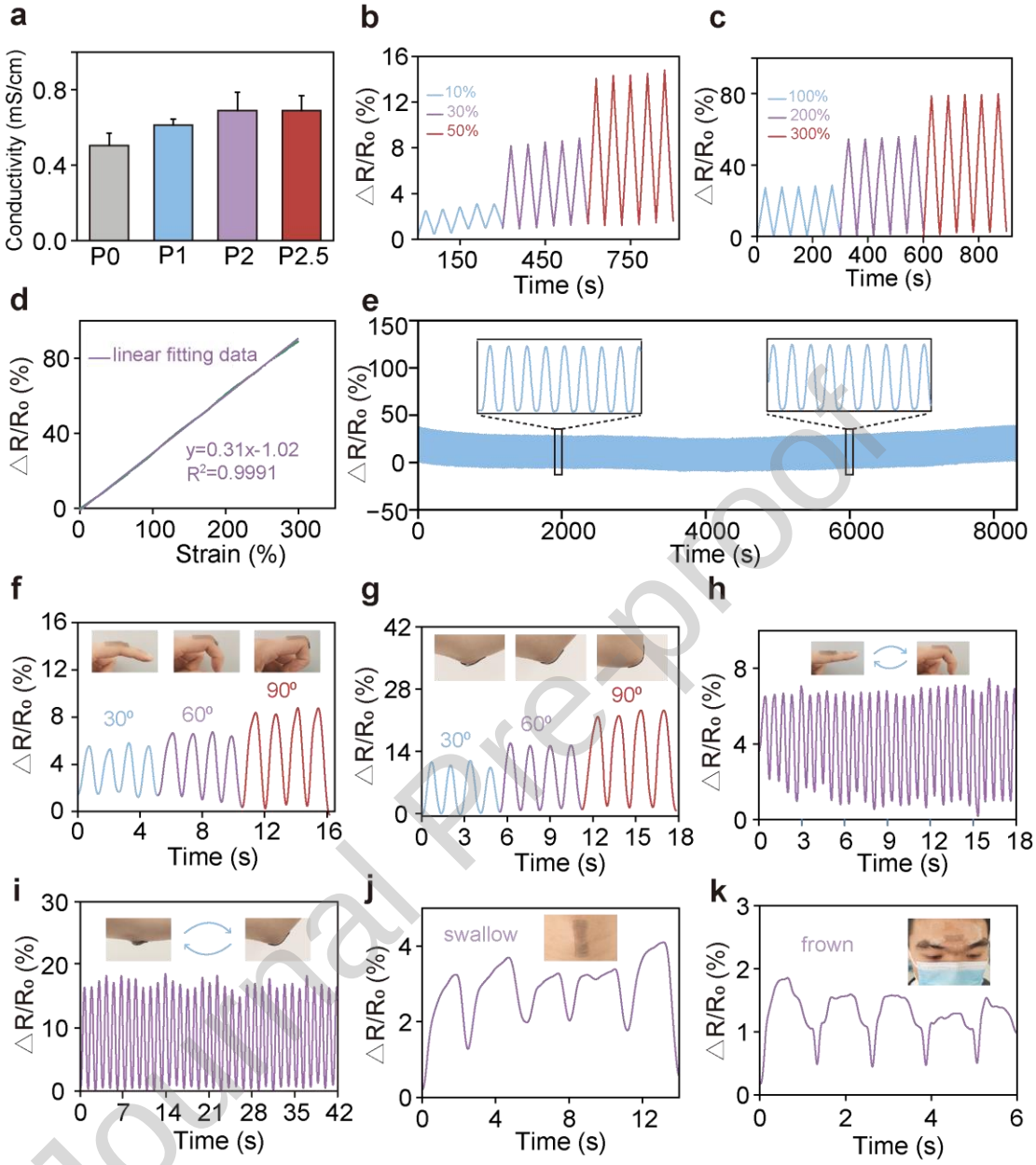

Fig. 5. PLOD adhered to the human body surface for motion detection. (a) Conductivity of PLOD. Rate of resistance change of PLOD under (b) small strain and (c) large strain. (d) Gauge factors of the PLOD. (e) Rate of resistance change of the PLOD for over 12000 tensile cycles under 100% strain with 1.5 Hz of frequency. (f) Finger bending at different angles. (g) Elbow bending at different angles. (h) Finger bending at 90° for various times. (i) Elbow bending at 60° for various times. (j) PLOD adhered to the neck to detect response to swallowing activity. (k) PLOD adhered to glabella to detect response to frowning activity.

3.5. Triboelectric nanogenerators based on PLOD nanocomposite hydrogel electrodes for tactile sensing

The high demand for flexible and self-powered supplies has driven research on soft and wearable TENGs, which can convert mechanical energy into electricity energy, enabling the fabrication of self-powered sensors [47]. However, traditional metal-based TENGs typically suffer from inferior stretchability, lack of self-healing, and tissue adhesion [48]. These shortcomings make them incompatible with stretchable materials, making it critical to develop new materials. In this work, we developed PLOD hydrogel as a conductive layer to serve as a potential platform for TENG tactile sensors. PDMS and PTFE were used as electrification layers, obtained using our previously reported method [49], and the PLOD served as electrodes. As shown in Fig. 6a, the electronegativity of PDMS was inferior to PTFE, contributing to a positively charged PDMS layer and a negatively charged PTFE layer, respectively. The opposite charges generated between the PLOD electrode and the PTFE triboelectric layer induced electron flow from the ground to PLOD electrode, creating a current from the PLOD electrode to the ground (Fig. 6ai). When PDMS made full contact with PTFE under an external force, the negative and positive charges on the PLOD electrode reached a state of equilibrium, and the flow of electrons and current stopped (Fig. 6aii). When the PDMS and PTFE were separated, a potential difference was induced between PLOD and the ground, causing the current to flow from the ground to the PLOD electrode (Fig. 6aiii). Afterwards, when the PTFE and PDMS were completely separated, the remaining charges gathered on the PLOD electrode (Fig. 6aiv). When PDMS had contact with PTFE again, the working mode returned to the initial state and then continued to circulate.

According to the above-mentioned model, a single-electrode mode PLOD-TENG was developed, and the PLOD-TENG generated acceptable output performance with an open-circuit voltage of about 13 V (Fig. 6b), short-circuit current of about 9 nA (Fig. 6c), and charge transfer amount of approximately 8 nC (Fig. 6d). Building on the sensitivity to external forces, a PLOD-TENG tactile sensing array was developed. The

fabrication process, illustrated in Fig. S18, began with a 3D-printed template mold, onto which PDMS was poured. After curing, the PDMS was detached from the mold to function as the substrate (Fig. S19). Prefabricated PLOD hydrogel lumps, as conductive units, were then fixed into the hollow vacancies by instant adhesive performance. After encapsulating with an additional layer of PDMS, the tactile sensing array was obtained, which carefully integrated nine 1×1 cm^2 TENG units into a 3×3 distributed sensing array, which was mounted on an FPCB (a type of flexible printed circuit board), with its copper coil removed and replaced with the PLOD. The sensing array could be comfortably and safely attached to the skin without causing discomfort or allergic reactions. As shown in Fig. 6e, f, the output waveform and voltage of each individual unit in the PLOD-TENG in the sensing array remained consistent under the same condition. Fig. 6h presents the interference tests, showing that users could touch any point on the sensing array, and the resulting voltage signals were recorded. The findings indicated that the sensing array could precisely identify a distinct signal of approximately 13 V at the target location, with adjacent sensors exhibiting at 2 V. In addition, the corresponding signal changes of sensors at different positions in the real-time interface were recorded (Fig. S20), despite the adjacent sensors around testing position also detected electrical signals, they do not cause interference, which implied that the recognition accuracy of signals activated by PLOD-TENG could be guaranteed by setting a reasonable trigger signal threshold.

The potential intelligent application of the sensing array was further investigated, as shown in Fig. 6g. The signal coding process primarily involved the sensing array action encoder, signal processing circuit, microcontroller, and intelligent application terminal. The touch and press interactions of the PLOD-TENG sensing array generated hybrid code groups that controlled specific operations. After the application of external force, the sensing array converted the mechanical signal into an electrical one, which was then processed by the microcontroller unit (MCU). The MCU pre-coded the PLOD-TENG sensing array behavior and compared it against a predefined threshold to determine whether the signal triggered an action, subsequently displaying

the corresponding effect on the PC terminal. A call system utilizing the PLOD-TENG sensing array action codes was developed for issuing medical warnings in healthcare institutions. As shown in Fig. 6i, each PLOD-TENG on the device could realize content-coded information, such as thirst, pain, and cold. When the corresponding unit in the PLOD-TENG sensing array was pressed, the corresponding content would display on the terminal, contributing to in-time management (Video S1, Supporting Information). Similarly, playing on an electronic keyboard was realized by using the PLOD-TENG sensing array developed in this work, as shown in Video S2.

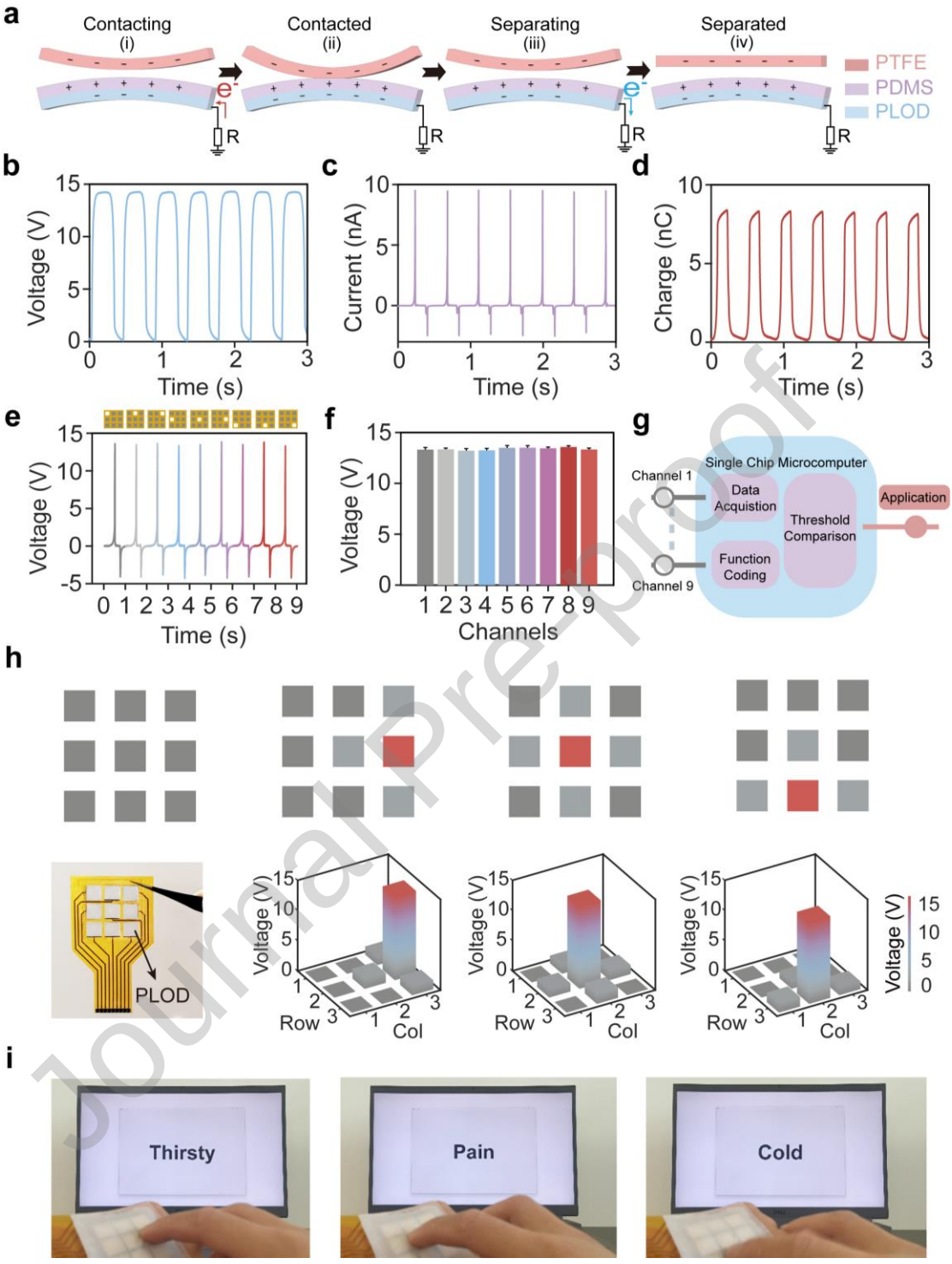

Fig. 6. PLOD-TENG sensing array for tactile sensing. (a) Schematic working principle for a single-electrode TENG. (b) Open-circuit voltage. (c) Short-circuit current, and (d) short-circuit charge of the TENG. (e) Output waveform of nine TENGs. (f) Output voltage of nine TENGs. (g) Schematic diagram of the human–computer interaction using PLOD-TENG sensing array. (h) 3D heat map

corresponding to different pressing positions on PLOD-TENG sensing array. (i) Application in call-in medical of the PLOD-TENG sensing array.

4. Conclusions

In this work, PLOD with stretchable, self-healing, tissue-adhesive, biocompatible, and electromechanical performance were successfully developed through the in situ gelation of an OEG methyl ether methacrylate monomer crosslinked with LAP and PEDOT:PSS. The LAP not only improved the colloidal stability of PEDOT:PSS through multi-scale interactions but also improved the stretching, conductivity, and strain sensing performance. The PLOD also exhibited excellent self-healing and adhesion properties due to their rich multiscale interactions, resulting in long-term functional stability and conformal interfaces. The PLOD also showed excellent electrical sensing performance and stability, which could be used to reliably and accurately monitor the different intensities of human body movements. In addition, the PLOD could be used as the flexible electrodes of TENGs. This PLOD-based interface engineering strategy offers significant promise for advancing the development and various applications of flexible wearable devices.

Declaration of Competing Interest

The authors declare that they have no known competing financial interests or personal relationships that could have appeared to influence the work reported in this paper.

Data availability

Data will be made available on request.

Acknowledgements

This study was supported by the National Natural Science Foundation of China grants (62461009 to Q.Z., 32360235 to L.J.T., T2125003 to Z.L.), the Guizhou Provincial Key Technology R&D Program (2024161 to Q.Z.), the Guizhou Provincial Basic Research Program (Natural Science) (ZK[2023]032 to Q.Z.; ZK[2022]-381 to L.J.T.), the Science and Technology Fund of Guizhou Provincial Health Commission

(gzwkj2022-444 to X.Y.Z.), the Youth Science and Technology Talents Growth Project of Guizhou Ordinary Colleges and Universities (KY[2024]100 to X.Y.Z.), the Youth Science and Technology Talent Development Project of Guizhou Medical University (22QNRC01 to L.J.T.). The authors also sincerely thank Dr. J. X. Chen at Key Laboratory of General Chemistry of the National Ethnic Affairs Commission, School of Chemistry and Environment, Southwest Minzu University for technical help with the Gaussian16 software calculations.

Author Contributions

X.Y.Z., L.J.T., X.P.W. and T.L contributed equally to this work. L.J.T., Z.Z., Z.Q.H., Z.L., and Q. Z. conceptualized and adapted the topics and experiments. X.Y.Z., L.J.T and X.P.W. made samples and carried out experiments. T.L. provided support for the guidance aimed at evaluating molecular reactivity and elucidating electron transfer mechanisms. Y.S.Z. W.L., D.L. and X.J.W processed the data. X.M.S., S.M.Z.,Y.D., and P.C.T. provided support for the guidance on creating a schematic diagram. X.Y.Z., L.J.T. completed the paper writing and was guided by Z.Z., Z.Q.H., Z.L., and Q.Z.

Appendix A. Supplementary data

Supplementary data to this article can be found online at xxxxxxxxxxx

References

[1] C. Xu, S.A. Solomon, W. Gao, Artificial intelligence-powered electronic skin, Nat. Mach. Intell. 5(12) (2023) 1344-1355, https://doi.org/10.1038/s42256-023-00760-z.

[2] W. Wang, D. Yao, H. Wang, Q. Ding, Y. Luo, H. Ding, J. Yu, H. Zhang, K. Tao, S. Zhang, A, F. Huo, J. Wu, A breathable, stretchable, and self-calibrated multimodal electronic skin based on hydrogel microstructures for wireless wearables, Adv. Funct. Mater. (2024) 2316339, https://doi.org/10.1002/adfm.202316339.

[3] Y. Li, D. Yang, Z. Wu, F.-L. Gao, X.-Z. Gao, H.-Y. Zhao, X. Li, Z.-Z. Yu, Self-adhesive, self-healing, biocompatible and conductive polyacrylamide nanocomposite hydrogels for reliable strain and pressure sensors, Nano Energy 109 (2023) 108324, https://doi.org/10.1016/j.nanoen.2023.108324.

[4] C. Hegde, J. Su, J.M.R. Tan, K. He, X. Chen, S. Magdassi, Sensing in soft robotics, ACS Nano 17(16) (2023) 15277-15307, https://doi.org/10.1021/acsnano.3c04089.

[5] H. Peng, Wearable electronics, Natl. Sci. Rev. 10(1) (2023) nwac193, https://doi.org/10.1093/nsr/nwac193.

[6] Q. He, Y. Cheng, Y. Deng, F. Wen, Y. Lai, H. Li, Conductive hydrogel for flexible bioelectronic device: current progress and future perspective, Adv. Funct. Mater. 34(1) (2024) 2308974, https://doi.org/10.1002/adfm.202308974.

[7] X. Yan, R. Zhao, H. Lin, Z. Zhao, S. Song, Y. Wang, Nucleobase-driven wearable ionogel electronics for long-term human motion detection and electrophysiological signal monitoring, Adv. Funct. Mater. (2024) 2412244, https://doi.org/10.1002 /adfm.202412244.

[8] Y. Wu, Y. Luo, T.J. Cuthbert, A.V. Shokurov, P.K. Chu, S.P. Feng, C. Menon, Hydrogels as soft ionic conductors in flexible and wearable triboelectric nanogenerators, Adv. Sci. 9(11) (2022) 2106008, https://doi.org/10.1002/advs.202106008.

[9] M. Yang, Y. Liu, G. Duan, Z. Liang, Y. Huang, C. Zhang, X. Han, C. Ma, S. He, S. Jiang, Recent advances of biomass-based smart hydrogel actuators: A review, Chem. Eng. J. (2024) 155157, https://doi.org/10.1016/j.cej.2024.155157.

[10] M. Xu, Y. Mao, W. Hu, All-hydrogel yarn-based supercapacitor wrapped with multifunctional cotton fiber for energy storage and sensing, Nano Energy 130 (2024) 110142, https://doi.org/10.1016/j.nanoen.2024.110142.

[11] X. Yang, B. Zhang, J. Li, M. Shen, H. Liu, X. Xu, S. Shang, Self-healing, self-adhesive, and stretchable conductive hydrogel for multifunctional sensor prepared by catechol modified nanocellulose stabilized poly (α-thioctic acid), Carbohydr. Polym. 313 (2023) 120813, https://doi.org/10.1016/j.carbpol.2023.120813.

[12] R. Li, J. Ren, M. Zhang, M. Li, Y. Li, W. Yang, Highly stretchable, fast self-healing, self-adhesive, and strain-sensitive wearable sensor based on ionic conductive hydrogels, Biomacromolecules 25(2) (2024) 614-625,

https://doi.org/10.1021/acs. biomac.3c0069 5.

[13] K. Tao, J. Yu, J. Zhang, A. Bao, H. Hu, T. Ye, Q. Ding, Y. Wang, H. Lin, J. Wu, Deep-learning enabled active biomimetic multifunctional hydrogel electronic skin, ACS Nano 17(16) (2023) 16160-16173, https://doi.org/10.1021/acsnano.3c05253.

[14] Y. Feng, S. Wang, Y. Li, W. Ma, G. Zhang, M. Yang, H. Li, Y. Yang, Y. Long, Entanglement in smart hydrogels: fast response time, anti-freezing and anti-drying, Adv. Funct. Mater. 33(21) (2023) 2211027, https://doi.org/10.1002/adfm.202211027.

[15] Z. Sun, C. Dong, B. Chen, W. Li, H. Hu, J. Zhou, C. Li, Z. Huang, Strong, tough, and anti-swelling supramolecular conductive hydrogels for amphibious motion sensors, Small 19(44) (2023) 2303612, https://doi.org/10.1002/smll.202303612.

[16] W.Y. Guo, M.G. Ma, Conductive nanocomposite hydrogels for flexible wearable sensors, J. Mater. Chem. A 12(16) (2024) 9371-9399, https://doi.org/10.1039/D3TA08069B.

[17] Z. Li, J. Lu, T. Ji, Y. Xue, L. Zhao, K. Zhao, B. Jia, B. Wang, J. Wang, S. Zhang, Self-healing hydrogel bioelectronics, Adv. Mater. 36(21) (2024) 2306350, https://doi.org/10.1002/adma.202306350.

[18] L. Teng, K. Xia, T. Qian, Z. Hu, L. Hong, Y. Liao, G. Peng, Z. Yuan, Y. Chen, Z. Zeng, Shape-recoverable macroporous nanocomposite hydrogels created via ice templating polymerization for noncompressible wound hemorrhage, ACS Biomater. Sci. Eng. 8(5) (2022) 2076-2087, https://doi.org/10.1021/acsbiomaterials.2c00115.

[19] P. Wei, T. Chen, G. Chen, H. Liu, I.T. Mugaanire, K. Hou, M. Zhu, Conductive self-healing nanocomposite hydrogel skin sensors with anti-freezing and thermoresponsive properties, ACS Appl. Mater. Interfaces 12(2) (2019) 3068-3079, https://doi.org/10.1021/acsami.9b20254.

[20] C. Tondera, T.F. Akbar, A.K. Thomas, W. Lin, C. Werner, V. Busskamp, Y. Zhang, I.R. Minev, Highly conductive, stretchable, and cell-adhesive hydrogel by nanoclay doping, Small 15(27) (2019) 1901406,

https://doi.org/10.1002/smll.201901406.

[21] Y. Li, X. Xiong, X. Yu, X. Sun, J. Yang, L. Zhu, G. Qin, Y. Dai, Q. Chen, Tough and conductive nanocomposite hydrogels for human motion monitoring, Polym. Test. 75 (2019) 38-47, https://doi.org/10.1016/j.polymertesting.2019.01.022.

[22] J. Yu, F. Tian, W. Wang, R. Wan, J. Cao, C. Chen, D. Zhao, J. Liu, J. Zhong, F. Wang, Design of highly conductive, intrinsically stretchable, and 3D printable PEDOT: PSS hydrogels via PSS-chain engineering for bioelectronics, Chem. Mater. 35(15) (2023) 5936-5944, https://doi.org/10.1021/acs.chemmater.3c00844.

[23] A. Shit, S.B. Heo, I. In, S.Y. Park, Mineralized soft and elastic polymer dot hydrogel for a flexible self-powered electronic skin sensor, ACS Appl. Mater. Interfaces 12(30) (2020) 34105-34114, https://doi.org/10.1021/acsami.0c08677.

[24] M. Xu, Q. Li, M. Xie, Y.-G. Jia, Y. Yang, Y. Chen, Engineering air-in-water emulsion as adaptable multifunctional sealant, Chem. Eng. J. 429 (2022) 132200, https://doi.org/10.1016/j.cej.2021.132200.

[25] M.J. Frisch, G.W. Trucks, H.B. Schlegel, G.E. Scuseria, M.A. Robb, J.R. Cheeseman, G. Scalmani, V. Barone, G.A. Petersson, H. Nakatsuji, X. Li, M. Caricato, A.V. Marenich, J. Bloino, B.G. Janesko, R. Gomperts, B. Mennucci, H.P. Hratchian, J.V. Ortiz, A.F. Izmaylov, J.L. Sonnenberg, D. Williams-Young, F. Ding, F. Lipparini, F. Egidi, J. Goings, B. Peng, A. Petrone, T. Henderson, D. Ranasinghe, V.G. Zakrzewski, J. Gao, N. Rega, G. Zheng, W. Liang, M. Hada, M. Ehara, K. Toyota, R. Fukuda, J. Hasegawa, M. Ishida, T. Nakajima, Y. Honda, O. Kitao, H. Nakai, T. Vreven, K. Throssell, J.A. Montgomery, Jr., J.E. Peralta, F. Ogliaro, M.J. Bearpark, J.J. Heyd, E.N. Brothers, K.N. Kudin, V.N. Staroverov, T.A. Keith, R. Kobayashi, J. Normand, K. Raghavachari, A.P. Rendell, J.C. Burant, S.S. Iyengar, J. Tomasi, M. Cossi, J.M. Millam, M. Klene, C. Adamo, R. Cammi, J.W. Ochterski, R.L. Martin, K. Morokuma, O. Farkas, J. B. Foresman, D.J. Fox, Gaussian 16, Revision B.01, Gaussian, Inc., Wallingford, CT, 2016.

[26] T. Lu, F. Chen, Multiwfn: A multifunctional wavefunction analyzer, J. Comput. Chem. 33(5) (2012) 580-592, https://doi.org/10.1002/jcc.22885.

[27] W. Humphrey, A. Dalke, K. Schulten, VMD: visual molecular dynamics, J. Mol. Graphics 14(1) (1996) 33-38, https://doi.org/10.1016/0263-7855(96)00018-5.

[28] X. Di, L. Li, Q. Jin, R. Yang, Y. Li, X. Wang, G. Wu, C. Yuan, Highly sensitive, degradable, and rapid self-healing hydrogel sensor with semi-interpenetrating network for recognition of micro-expressions, Small (2024) 2403955, https://doi.org/10.1002/ smll.202403955.

[29] X. Han, C. Saengow, L. Ju, W. Ren, R.H. Ewoldt, J. Irudayaraj, Exosome-coated oxygen nanobubble-laden hydrogel augments intracellular delivery of exosomes for enhanced wound healing, Nat. Commun. 15(1) (2024) 3435, https://doi.org/10.1038 /s41467-024-47696-5.

[30] H. Zheng, N. Lin, Y. He, B. Zuo, Self-healing, self-adhesive silk fibroin conductive hydrogel as a flexible strain sensor, ACS Appl. Mater. Interfaces 13(33) (2021) 40013-40031, https://doi.org/10.1021/acsami.1c08395.

[31] M. Shan, X. Chen, X. Zhang, S. Zhang, L. Zhang, J. Chen, X. Wang, X. Liu, Injectable conductive hydrogel with self-healing, motion monitoring, and bacteria theranostics for bioelectronic wound dressing, Adv. Healthcare Mater. 13(11) (2024) 2303876, https://doi.org/10.1002/adhm.202303876.

[32] Z. Chen, J. Yang, Z. Du, J. Ji, L. Zhang, H. Guan, Z. Lei, X. Zhang, C. Yang, Y. Zhu, A conductive and anti-freezing gelatin-PAA-based organic hydrogel (PC-OH) with high adhesion and self-healing activities for wearable electronics, Chem. Eng. J. 492 (2024) 152465, https://doi.org/10.1016/j.cej.2024.152465.

[33] H. Sun, Y. Han, M. Huang, J. Li, Z. Bian, Y. Wang, H. Liu, C. Liu, C. Shen, Highly stretchable, environmentally stable, self-healing and adhesive conductive nanocomposite organohydrogel for efficient multimodal sensing, Chem. Eng. J. 480 (2024) 148305, https://doi.org/10.1016/j.cej.2023.148305.

[34] M. Li, A. Mao, Q. Guan, E. Saiz, Nature-inspired adhesive systems, Chem. Soc. Rev. (2024), https://doi.org/10.1039/D3CS00764B.

[35] B. Xie, Y. Ma, N. Luo, Y. Chen, Y. Liu, K. Nie, Y. Jia, R. Yin, Y. Liu, Triple network hydrogel-based structure triboelectric nanogenerator for human motion detection and structural health monitoring, Nano Energy 130 (2024) 110095,

https://doi.org /10.1016 /j.nanoen.2024.110095.

[36] S. Guo, Y. Park, E. Park, S. Jin, L. Chen, Y.M. Jung, Molecular-orbital delocalization enhances charge transfer in π-conjugated organic semiconductors, Angew. Chem., Int. Ed. 62(34) (2023) e202306709, https://doi.org/10.1002/anie.202306709.

[37] P. Gurnani, G.R. Williams, Investigating oligo (ethylene glycol) methacrylate thermoresponsive copolymers, Eur. Polym. J. 216 (2024) 113266, https://doi.org/10.1016/j.eurpolymj.2024.113266.

[38] Q. Gao, C. Li, M. Wang, J. Zhu, C. Gao, A low-hysteresis, self-adhesive and conductive PAA/PEDOT: PSS hydrogel enabled body-conformable electronics, J. Mater. Chem. C 11(27) (2023) 9355-9365, https://doi.org/10.1039/D3TC00850A.

[39] W. Wang, Y. Chen, C. Xiao, S. Xiao, C. Wang, Q. Nie, P. Xu, J. Chen, R. You, G. Zhang, Flexible SERS wearable sensor based on nanocomposite hydrogel for detection of metabolites and pH in sweat, Chem. Eng. J. 474 (2023) 145953, https://doi.org/10. 1016/j.cej.2023.145953.

[40] W. Xia, Y. Yu, C. Zhou, W. Wang, Z. Wu, H. Chen, Itaconic acid-enhanced robust ionic conductive elastomers for strain/pressure sensors, J. Mater. Chem. C 11(47) (2023) 16545-16553, https://doi.org/10.1039/D3TC03708H.

[41] X. Pei, H. Zhang, Y. Zhou, L. Zhou, J. Fu, Stretchable, self-healing and tissue-adhesive zwitterionic hydrogels as strain sensors for wireless monitoring of organ motions, Mater. Horiz. 7(7) (2020) 1872-1882, https://doi.org/10.1039/D0MH00361A.

[42] Y. Zheng, A. Baidya, N. Annabi, Molecular design of an ultra-strong tissue adhesive hydrogel with tunable multifunctionality, Bioact. Mater. 29 (2023) 214-229, https://doi.org/10.1016/j.bioactmat.2023.06.007.

[43] W. Li, X. Yang, P. Lai, L. Shang, Bio-inspired adhesive hydrogel for biomedicine—principles and design strategies, Smart Med. 1(1) (2022) e20220024, https://doi.org/10.1002/SMMD.20220024.

[44] S. Murugesan, T. Scheibel, Copolymer/clay nanocomposites for biomedical

applications, Adv. Funct. Mater. 30(17) (2020) 1908101, https://doi.org/10.1002/adfm.201908101.

[45] D. Zhang, Y. Tang, Y. Zhang, F. Yang, Y. Liu, X. Wang, J. Yang, X. Gong, J. Zheng, Highly stretchable, self-adhesive, biocompatible, conductive hydrogels as fully polymeric strain sensors, J. Mater. Chem. A 8(39) (2020) 20474-20485, https:// doi.org/10.1039/D0TA07390C.

[46] Z. Li, C. Li, W. Sun, Y. Bai, Z. Li, Y. Deng, A controlled biodegradable triboelectric nanogenerator based on PEGDA/laponite hydrogels, ACS Appl. Mater. Interfaces 15(10) (2023) 12787-12796, https://doi.org/10.1021/acsami.2c22359.

[47] F.R. Fan, Z.Q. Tian, Z.L. Wang, Flexible triboelectric generator, Nano energy 1(2) (2012) 328-334, https://doi.org/10.1016/j.nanoen.2012.01.004.

[48] Z. Jin, F. Zhao, Y. Lei, Y.C. Wang, Hydrogel-based triboelectric devices for energy-harvesting and wearable sensing applications, Nano Energy 95 (2022) 106988, https://doi.org/10.1016/j.nanoen.2022.106988.

[49] X. Wu, Z. Yang, Y. Dong, L. Teng, D. Li, H. Han, S. Zhu, X. Sun, Z. Zeng, X. Zeng, A self-powered, skin adhesive, and flexible human–machine interface based on triboelectric nanogenerator, Nanomaterials 14(16) (2024) 1365, https://doi.org/ 10.3390/nano14161365.

Declaration of interests

The authors declare that they have no known competing financial interests or personal relationships that could have appeared to influence the work reported in this paper.

Highlights

- Multiple physically crosslinked nanocomposite hydrogels were developed

through in situ doping of poly(3,4-ethylenedioxythiophene):poly(styrenesulfonate) in a Laponite® crosslinked oligo ethylene glycol (OEG) methyl ether methacrylate copolymer.

- This nanocomposite hydrogel exhibits excellent stretchability, high self-healing efficiency, robust tissue adhesion, and good biocompatibility.
- This nanocomposite hydrogel can be used as a skin conformal strain sensor for human motion monitoring.
- This nanocomposite hydrogel can be used as a flexible electrode of triboelectric nanogenerator, enabling tactile sensing for human-machine interaction